WEAK MOTION ATTENUATION OF PEAK GROUND ACCELERATION IN THE NORTH ISLAND, NEW ZEALAND

Aasha Pancha[1] and John Taber[2]

ABSTRACT

Attenuation relations using weak ground motion recordings have been determined using data from the New Zealand National Seismograph Network and several temporary seismograph deployments. Models have been developed for earthquake sources in four regions: the Eastern North Island deep and shallow regions and the Central North Island (CNI) deep and shallow regions. Deep events were those with hypocenters below 33 km. Regression coefficients have been determined using the attenuation models of Joyner and Boore (1981) and Molas and Yamazaki (1995).

The anelastic attenuation rates in the Eastern North Island expressions are comparable to that of Joyner and Boore (1981), suggesting that weak motion attenuation can be used to estimate variations in strong motion attenuation. However, the absolute level of the strong-motion attenuation curves greatly differs from those of the weak-motion.

The anelastic attenuation rate for the shallow CNI is of the order of two to three times that observed for the Eastern North Island. The lowest attenuation rate was found for events within the deep CNI, whose ray paths did not cross the shallow Central North Island region. This is consistent with a low rate of attenuation in the subducting Pacific plate.

Azimuthal dependence of PGA is evident within each of the regions. Within the Eastern North Island, the attenuation rate is lowest in the direction of 35-55° from North, which is roughly along the strike of the subducting Pacific plate. A similar azimuthal dependence was also noted within the deep CNI region, while a slightly different minimum direction (5°) was determined for the shallow CNI region.

INTRODUCTION

An accurate attenuation model is a crucial element of any seismic hazard study, as both design parameters and damage estimates are heavily influenced by the choice of attenuation model. In the past, models from either Japan or the US have been used in New Zealand because of insufficient local strong motion data. A best-average New Zealand peak ground acceleration attenuation model has recently been developed by Zhao *et al.* (1997) based on the available strong-motion data, but while regional variations were noted, they had insufficient data to define regional attenuation relations.

This paper describes the use of the digital weak-motion database of the New Zealand National Seismic Network (NZNSN) to determine the attenuation of peak ground acceleration (PGA) on a finer scale than is possible with the strong motion data. The aim of this study is to use the weak-motion database to map spatial changes in attenuation within the North Island of New Zealand. While the motions considered are far below damaging levels, the variations in attenuation may have a bearing on strong-motion models. Most NZNSN stations are sited on bedrock, so the attenuation should be less contaminated by geological site effects. This is in contrast to the strong motion network which tends to be concentrated in population centres and therefore samples a wide range of site conditions.

[1] *Institute of Geological & Nuclear Sciences, Lower Hutt*

[2] *Victoria University of Wellington, Member*

Most PGA studies in New Zealand have made comparisons to overseas attenuation curves, particularly the western US (Joyner and Boore, 1981; Campbell, 1981) or Japan (Fukushima and Tanaka, 1990; Molas and Yamazaki, 1995), because of the limited strong motion data in New Zealand. Dowrick and Sritharan (1993a, b) concluded that for events in all areas but Fiordland, there is a reasonable fit to the Japanese models, but the PGA's are much higher than that predicted by the western US models.

Most recently Zhao *et al.* (1997) developed attenuation relations for PGA for New Zealand earthquakes of M_w = 5.1 - 7.4. Regional differences of PGA attenuation rates for Fiordland and the Central Volcanic Region (CVR) compared to the rest of New Zealand were investigated. Data from Fiordland events suggest that PGA's in this region are higher for a given set of parameter values than elsewhere in the country. Travel paths within the CVR were found to experience a higher rate of attenuation than other areas of New Zealand but there were insufficient data to determine regression parameters.

Many studies of attenuation in New Zealand have used intensity data because it was available for the largest events. Smith (1978, 1995) separated New Zealand into three separate regions, the eastern North Island, Fiordland and the remainder of New Zealand, each with its own set of attenuation curves. He also defined the ellipticity of the isoseismals for each region. Dowrick (1991) revised the attenuation relationships using new magnitudes and included a depth factor. He used circular isoseismals and did not find a regional variation in attenuation except for the CVR and perhaps Fiordland. The differences in the Smith and Dowrick models have important implications for seismic hazard assessment, particularly whether there are azimuthal and regional variations in intensity. Satake and Hashida (1989) inverted for the 3D attenuation structure of the North Island using intensities. They found a low Q in the CVR and a high Q in the subducting slab.

New Zealand was also divided into a small number of regions based on the amplitude attenuation studies of Haines (1981). Ray paths for crustal earthquakes were assigned the same attenuation unless they traversed the CVR. Subcrustal earthquakes were divided into 2 groups: the main seismic zone and the region to the south of the main seismic zone.

This paper, which is based on Aasha Pancha's MSc thesis research (Pancha, 1997), addresses the variability of attenuation relations within the Eastern North Island (ENI) and the Central North Island (CNI) regions of New Zealand. The data selection and processing will be described followed by an explanation of the form of the attenuation relations used in the study. Then the results of the regression analyses and their implications will be discussed, including the consideration of azimuthal effects.

DATA SELECTION

Earthquakes recorded by the New Zealand National Seismograph Network from 1993-1994 were considered for the analysis. This time interval occurs after the network was upgraded to digital recording. As seen in Figure 1, the station distribution is rather sparse with an average spacing of about 100 km. To increase the density of attenuation data in the mid-field region, recordings from temporary deployments operated by the Institute of Geological and Nuclear Sciences (IGNS) were included in the data set. These include the East Cape and Marlborough deployments in 1993-1994, and the Taupo Volcanic Zone deployment in 1995. Station spacing within the temporary deployments was about 10-50 km. Figure 2 shows the location and distribution of stations of these three main temporary deployments. However, as later discussed, some of the data from these deployments were excluded from the final regressions.

Earthquakes from the IGNS National Catalogue were considered if their local magnitude (M_L) was > 3.0 and their location was within the Eastern North Island (ENI) or Central North Island region (CNI). The regions are based roughly on the seismicity "Regions C and D" defined by Smith and Berryman (1983) (Figure 1). The CNI region, however, extends beyond the CVR to include earthquakes to the south-west. Within each region, data were classified as either shallow ($\leq$ 33 km) or deep. Thus the data were separated into four different regions for analysis: the Eastern North Island shallow (ENIS); Eastern North Island deep (ENID); Central North Island shallow (CNIS); and Central North Island deep (CNID).

Events were selected if they were recorded on a large number of three component stations, either because of their large magnitude or because of their proximity to a dense portable deployment. Locality of events was a secondary criterion for data selection to ensure data were well distributed spatially within each region.

In total, 109 events were analysed: 31, 25, 23 and 29 events respectively for the CNI deep, CNI shallow, ENI deep and ENI shallow regions. Figure 3 shows the event distribution for each of these regions. Events have not been classified on the basis of source mechanism because the mechanisms for most of the events used in this project have not been determined. This lack of classification will add to the scatter of the data as source mechanisms have been shown to be a factor in PGA (Dowrick and Sritharan, 1993a, b; Zhao *et al.*, 1997).

DATA PROCESSING

Waveforms from the selected events were first extracted from the IGNS earthquake catalogue. The processing steps included converting between data formats (CUSP to AH), removing the instrument response of the velocity sensor, and then converting from velocity to acceleration. Only sites with EARSS recording systems (Gledhill *et al*, 1991) were considered so that the system response was the same for all sites, and only horizontal components were considered because of the greater engineering significance of horizontal motions.

In converting the waveform data to accelerations, the traces were de-meaned and tapered using a 10% parzen taper. The instrument response was then removed from each of the waveforms. The deconvolution included a third order high

pass filter at 0.5 Hz. Following the removal of the instrument response the waveforms represented the ground velocity. The waveforms were then once again tapered and the derivative of the velocity function was computed by the spectral method to obtain acceleration traces in m/sec^2. A low-pass 25 Hz butterworth filter was then applied.

Once this processing had been completed, each individual trace was viewed to ensure that the maximum value was the true maximum acceleration and that the traces were not dominated by noise. If traces included constant background noise or noise spikes which overshadowed the true value, the trace was eliminated. Stations with a signal to noise ratio of less than four were also eliminated. The NZNSN stations used have a sampling rate of 50 Hz while the temporary deployment stations had a sampling rate of 100 Hz.
The peak value of each horizontal component was read and both the maximum of the two components and root mean squared value of the two components for each station were tabulated. Figure 4 shows plots of the distance distribution versus maximum PGA for the four regions of this study. At large distances the data become sparse. For this reason, and to minimise bias due to untriggered (null observations) and non-operational stations, data for each of the four regions were truncated at a distance of 500 km. As discussed later, the data was further reduced after initial analysis revealed that data from some of the temporary deployments were too highly scattered.

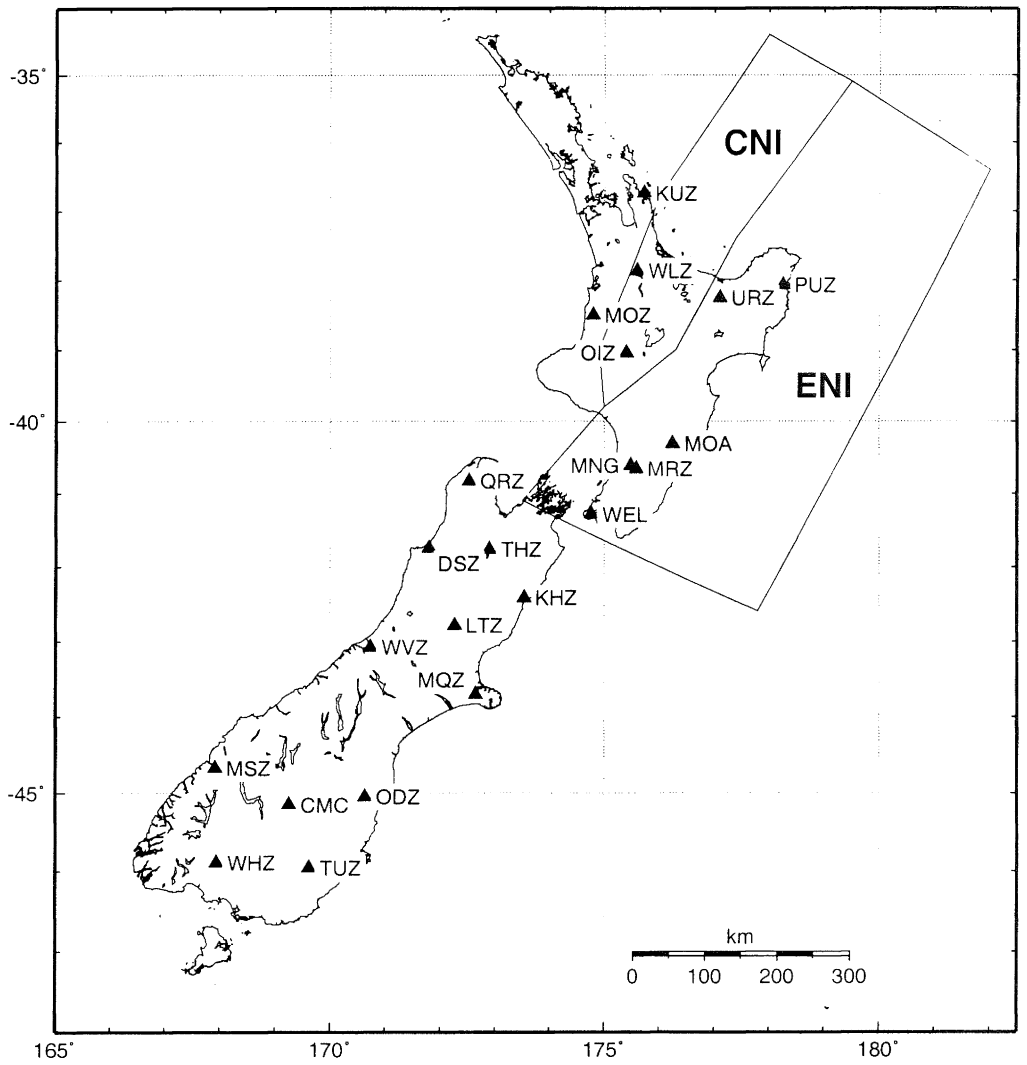

Figure 1: New Zealand National Seismograph Network. Map showing locations of the three component EARSS digital stations installed during the time interval of this study. The location of the Eastern North Island (ENI) and Central North Island (CNI) regions are superimposed. The regions are based roughly on the seismicity regions of Smith and Berryman (1983).

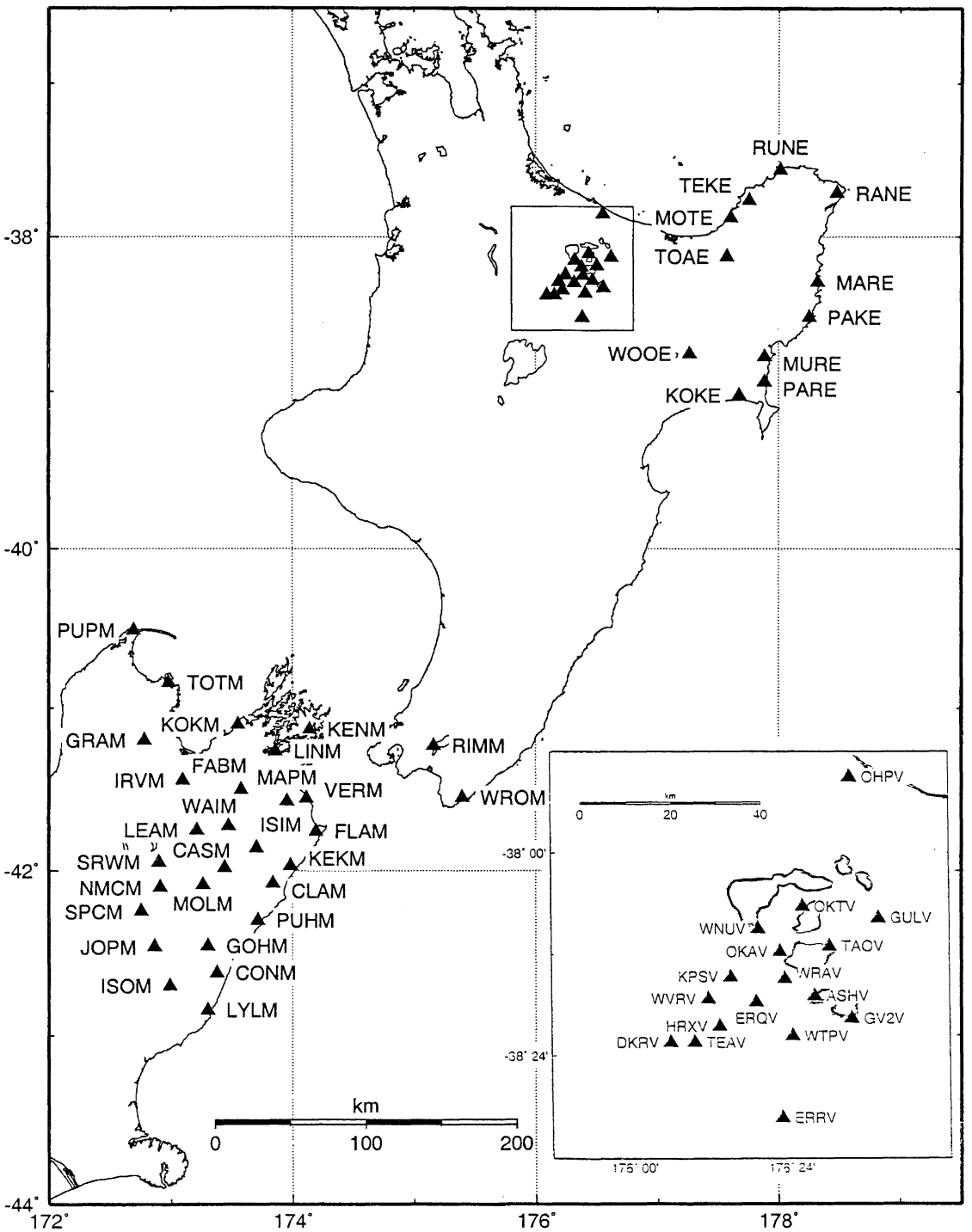

Figure 2: Map showing station location and stations of the three main portable deployments: the East Cape, Marlborough, and the Taupo Volcanic Zone (inset). Only the stations which are mentioned within this paper are shown.

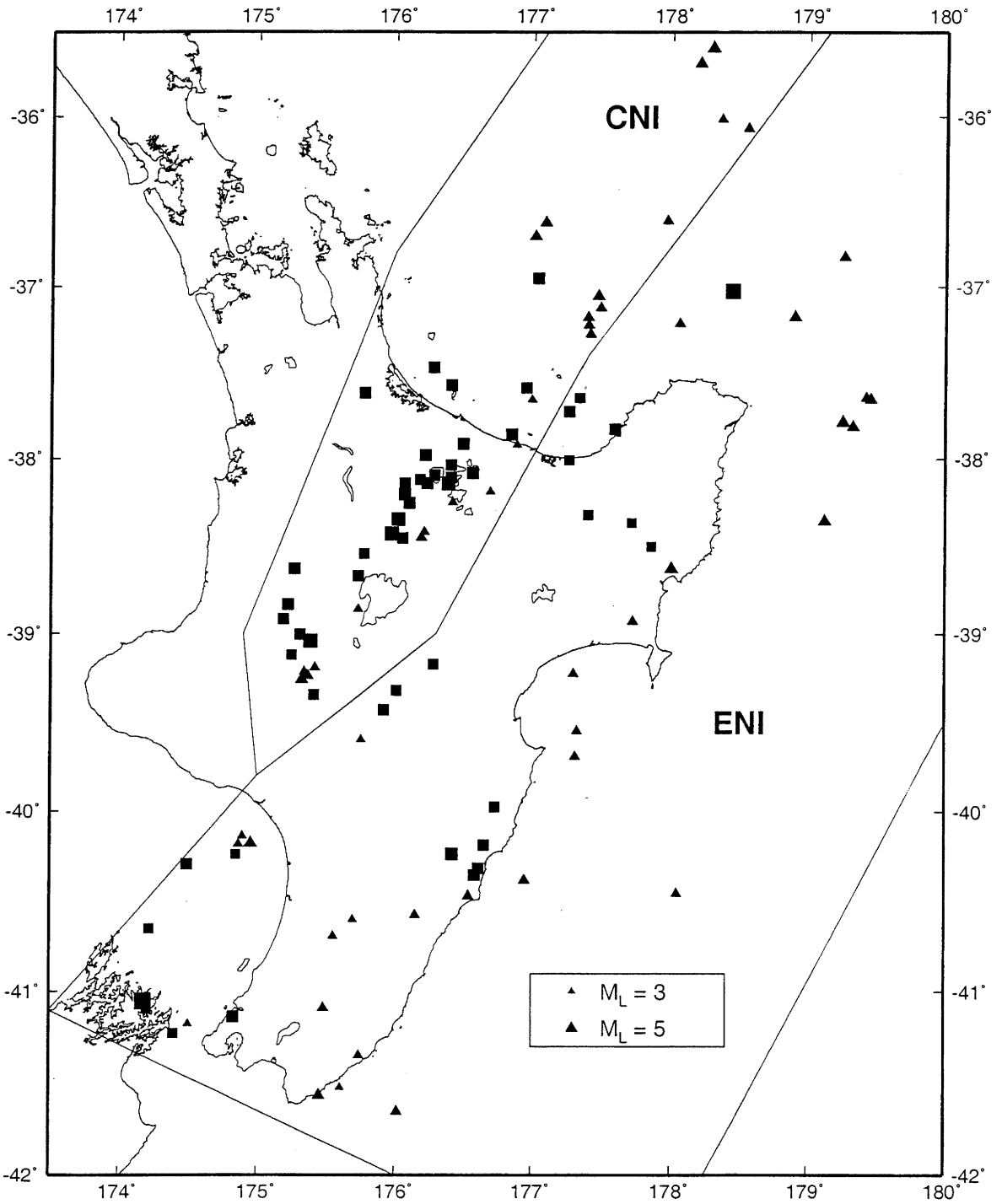

Figure 3: Earthquake locations within the Central and Eastern North Island regions. Boundaries of the two regions are also shown. Events deeper than 33 km are represented by a square, while shallow earthquakes are represented by a triangle. Symbols are scaled by magnitude.

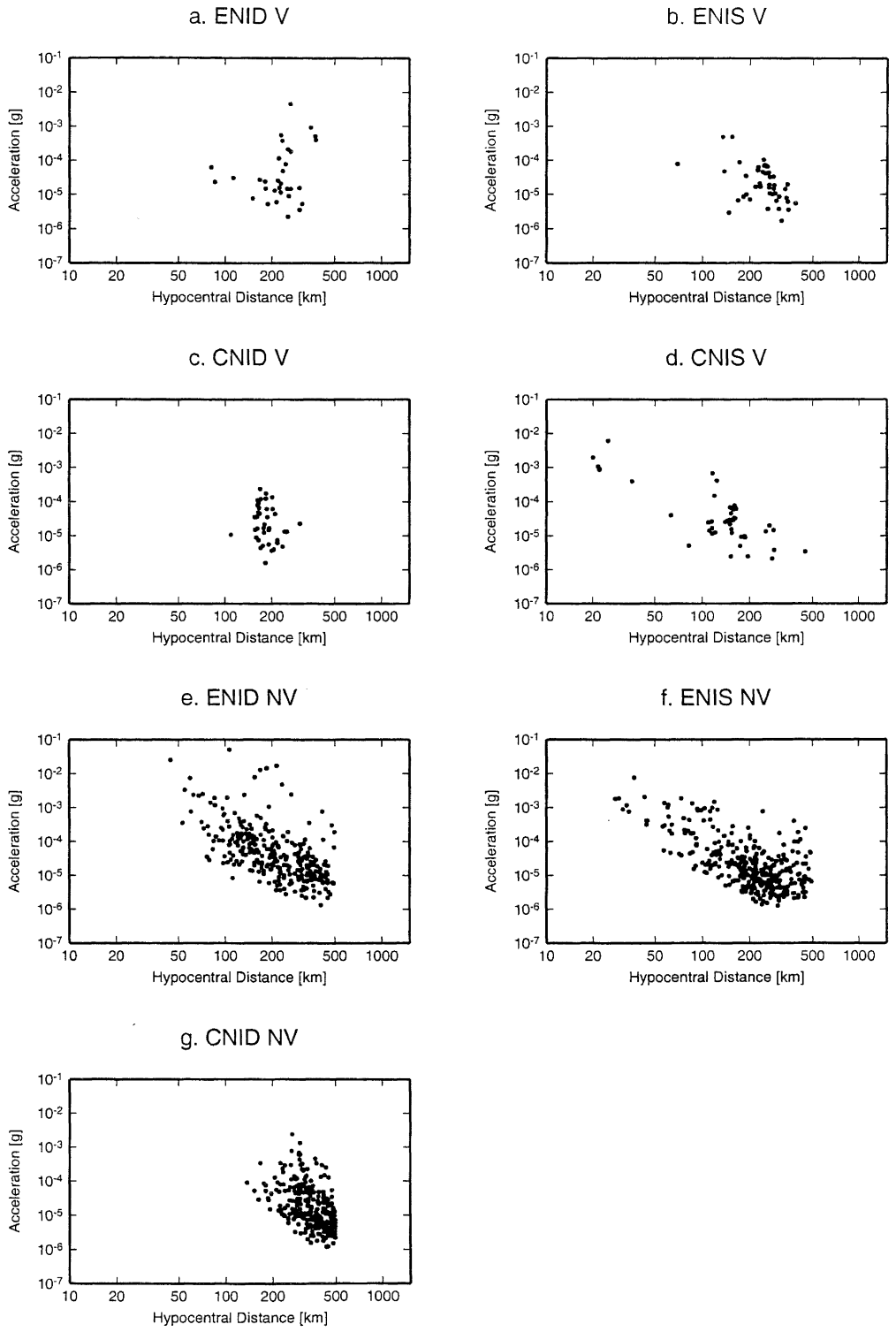

Figure 4: Distribution of acceleration data with distance within each of the four regions for both the non-volcanic (NV)(no part of the ray path within the CNI) and volcanic (V) data sets. Hypocentral distances are shown. CNID = Central North Island (Deep); CNIS = Central North Island (Shallow); ENID = Eastern North Island (Deep); ENIS = Eastern North Island (Shallow). Data beyond 500 km were not used in the regressions.

ACCELERATION COMPARISONS

It was necessary to ensure that the conversion of the CUSP velocity data to acceleration was in agreement with the acceleration measured on strong motion instruments. In order to do this, comparisons between earthquake data recorded simultaneously on an EARSS seismograph and an adjacent strong-motion accelerograph were made independently by IGNS and in the current study. The instruments were operated by IGNS at the Seismological Observatory, Kelburn for a five month period. Six events were used in the comparison.

In this study, the seismograph data were processed in the same manner as that of the main data set. The resultant PGA values were compared with those of the accelerograph which were supplied by IGNS. At most, discrepancies between the two values of PGA were within 12% of each other with five of the six measurements having less than 5% difference. A similar comparison was made of data from weight drops at the new Museum of New Zealand site, Wellington, where a difference of at most 10% was observed.

The processing methods used by IGNS gave very similar values of acceleration to the current study with at most a 5% difference. IGNS also compared a data set of 295 rock-site PGA's from seismograms recorded between 1990 and 1995 with strong-motion rock-site data. Statistical analyses of these two data sets showed that the variance of the seismograph rock-site data was greater than that of the strong-motion data from all sites (Jim Cousins, personal communication, 1996).

The above analyses demonstrate that PGA derived from the conversion of velocity data from the NZNSN are comparable to the PGA determined from strong ground motion instrumentation.

REGRESSION ANALYSIS

For this study of far-field, weak motion attenuation, the models and methods of Joyner and Boore (1981) and Molas and Yamazaki (1995) have been adopted. The Joyner and Boore (1981) model was selected because it is based on the attenuation of body waves in an elastic medium from a point source. The Molas and Yamazaki (1995) model was chosen for the same reason, and because it includes both a depth term and a constant term for each recording station. Moreover, Molas and Yamazaki (1995) used data from Japan, which has a similar tectonic environment to New Zealand.

The Joyner and Boore Two Stage Regression:

The two stage regression of Joyner and Boore (1981) (hereafter JB) is the primary technique used for deriving attenuation models in this study. The technique was favoured because of its simple model and because the method decouples the distance dependence from the magnitude dependence using a two-stage regression.

The Joyner and Boore model is as follows:

$$\log_{10} y = c + a M + br - \log_{10} r + d S ,$$

where $r = (d^2 + 7.3^2)^{1/2}$ and d is the shortest distance to the projection of fault rupture and y is the acceleration in g. In the current study, which uses events at larger distances and greater depths than the JB model, r is taken as the hypocentral distance in kilometers. The station term, S, equals zero as all stations are located on bedrock. The $\log_{10} r$ term accounts for geometric spreading while br is the anelastic attenuation term. JB use the two stage regression to determine the coefficients in order to separate the magnitude dependence from the distance dependence. In the first stage, values for the distance coefficient and a constant term for each earthquake are determined from the acceleration data using dummy variables (Draper and Smith, 1981). The earthquake terms are then regressed against magnitude in the second stage to determine the magnitude coefficients and the constant term.

The Molas and Yamazaki Regression Model and Method:

In addition to the JB attenuation model, the regression model and method of Molas and Yamazaki (1995) (hereafter MY) was applied. The form of their model is as follows:

$$\log_{10} y = b_0 + b_1 M + b_2 r + b_3 \log_{10} r + b_4 h + c_i,$$

where

y	=	acceleration in cm/s^2.
M	=	is the magnitude.
r	=	is the shortest distance to the fault surface, where known, otherwise the hypocentral distance in km.
h	=	is the depth in km.
c_i	=	is the station coefficient of the i th recording station.

MY employ a three stage technique, similar to the two stage approach of JB. In addition to the terms adopted by JB, MY include a depth term and station terms which are also calculated through the use of dummy variables. From preliminary analyses, MY showed that both the depth term and the station term significantly improved the fit of the regression model. A positive correlation between the residuals and depth were noted when the depth term was omitted. When the depth term was incorporated, the R^2 statistic significantly improved and the standard error reduced.

Although the recording stations of this study are located on bedrock, local geological and topographic variations can result in differences in site amplification. Thus to gain a better fit to the attenuation data and a better understanding of recording site influences, the inclusion of a station term for this study was desirable.

PARAMETERS

Two definitions of the independent variable, the horizontal acceleration, have been regressed for. Traditionally peak

ground acceleration is usually preferred (e.g. Joyner and Boore, 1981; Bolt and Abrahamson, 1982; Ambraseys and Bommer, 1991; Molas and Yamazaki, 1995). However, peak values often vary greatly between the orthogonally oriented horizontal components. For this reason the regressions were also determined using the root-mean-squared of the peak values of the two horizontal components. No significant difference between the two measures of acceleration was noted. All calculations presented in this paper are therefore derived using the maximum peak ground acceleration of the two components.

The distance between the recording sites and the energy source of the weak motion is generally of the order of 100 km or more. Unlike strong motion studies, this removes the problem of stations being closer to some part of the fault rupture than the initiation of energy release. As a result, the hypocentral distance, as calculated from the IGNS catalogue location, has been used in this study.

Since 1977, New Zealand earthquakes have been classified using a local magnitude scale. The scale is a revised definition of Richter's original scale based on the characteristics of seismic attenuation beneath New Zealand (Haines, 1981). Hence, M_L has been adopted as a measure of earthquake size throughout this study as values were available for all weak motion events, whereas M_W and M_S values are only available for selected strong motion events.

REGRESSION RESULTS AND DISCUSSION

Initial analysis of the data from each of the four regions revealed that data related to temporary deployments, and in particular, the East Cape and Taupo Volcanic Zone deployments were associated with a large degree of scatter. Over small distance ranges, data from these deployment stations had a large variation in PGA (e.g. Figure 5). This was not totally unexpected. While stations of the NZNSN are located on the hardest rock type within the region, those of the short term deployments are less likely to be. As a result, site conditions vary greatly from station to station. This may give rise to the scatter observed. The same effect is not noted within the Marlborough deployment, probably because these stations are situated on older, higher grade metamorphic rocks. These rocks are more consolidated than the sedimentary and volcanic deposits within the Eastern North Island and Taupo Volcanic regions. Preliminary analysis also revealed that attenuation station terms for stations of the East Cape deployment, derived using the MY model, exhibit much less variation than seen in an individual event (Pancha, 1997). This implies that the scatter must be at least partially a path effect and not solely a site effect. No correlation between the azimuth of the earthquake events and the observed deviation is noted. It is clear that some regional effect is influencing the attenuation of seismic waves travelling into this area. This effect may perhaps be due to a sediment package within the accretionary wedge along the plate interface. In order to separate the contribution of site effects from path effects, a more in-depth analysis of the ray paths would be required. However, as these widely scattered data values of the East Cape and Taupo Volcanic Zone deployment stations greatly influenced the regression relations they were therefore removed.

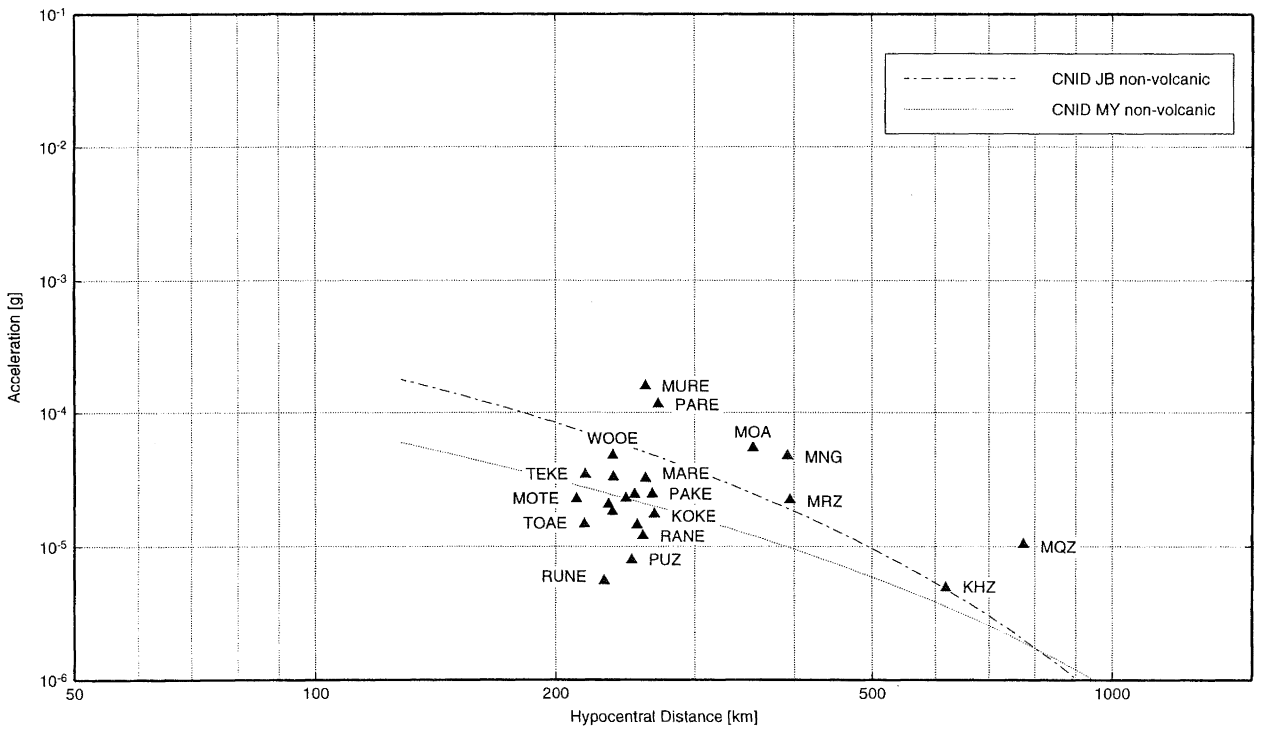

Figure 5: Comparison of derived CNID attenuation relations with a CNID event of M_L = 4.2 and depth = 182 km. Note the scatter of data from the East Cape Deployment stations (stations ending in "E"). The non-volcanic attenuation curves were derived by excluding the East Cape Deployment stations and stations with ray paths through the CNI.

Data from the East Cape deployment and most of the Taupo Volcanic Zone deployment were removed from each of the data sets. The data sets for each of the four regions were then further divided, each data set being separated into two classes. The first class comprised data which had not experienced attenuation effects of the shallow CNI region. It included stations from the Marlborough deployment as well as most of the NZNSN stations. The NZNSN stations KUZ, MOZ, OIZ, WLZ, and those of the Taupo Volcanic Zone deployment were eliminated as any waves travelling to these stations must pass through the Central Volcanic Region. This data set is hereafter referred to as the "non-volcanic" data set. Note that there is no CNIS region for this data set.

The second class comprised earthquake recordings for which ray paths pass through the Central North Island region. Thus the data is referred to as the "volcanic" data set. Recording stations of this class included the four NZNSN stations, KUZ, MOZ, OIZ and WLZ, as well as three of the Taupo Volcanic Zone deployment stations (DKRV, GV2V and OKAV). Only three stations from the deployment were selected because of the problem of scatter. The three stations were chosen because they seem to be more consistent, and because they recorded a larger number of the events than other stations within the deployment. The distribution of both data sets are shown in Figure 4 and Table 1.

Regressions using both the JB model as well as the MY model were performed on the non-volcanic data set. As some events only contained one data record, these were removed from the magnitude dependent regressions following the procedure of JB. The resultant attenuation models are shown in Table 2.

One expects that the anelastic attenuation term (the distance term) will increase with increasing attenuation along the ray path. Anelastic losses are greatest in the shallow section of the crust (Atkinson, 1995). We therefore expect that the relations obtained for the shallow data subsets will yield anelastic attenuation coefficients (coefficient of r (b and b_2) in Table 2) that are larger (more negative) than those of the deep data subsets. From Table 2 we see that the anelastic coefficient of the ENI data is significantly larger than that for the CNID, as expected.

The rates of anelastic attenuation in the ENIS and ENID regions are the same for the JB technique, and are similar to those obtained using the MY method. Thus for the distances considered in this study, the rate of attenuation from earthquakes occurring in the upper 33 km of the crust is comparable to that of earthquakes occurring below 33 km within the Eastern North Island region. Attenuation rates of the CNID, where earthquakes originated within the subducting slab, are much less. This confirms the observation that seismic waves travelling through the subducting Pacific Plate experience much less attenuation than those travelling through the overlying crust (Satake and Hashida, 1989).

It has been known that attenuation rates within the Central Volcanic Region are high (e.g. Mooney, 1970; Hatherton, 1970; Zhao *et al.*, 1997). Regression analyses using only those records from the volcanic data set that had travelled through the CNI region, allowed the influence of the CVR to be quantified. Because the resulting subsets were so sparse, only the first stage of the traditional JB method was applied to gain the anelastic attenuation rate (Table 3). As expected, the anelastic attenuation is greater for ray paths that pass through the CNI, compared to the rates derived for ray paths through the subducting slab and the rest of the overlying Australian Plate (Table 2). Waves travelling from the Eastern North Island regions into the shallow CNI and from the CNID up to the shallow CNI have a similar anelastic attenuation rate as waves travelling solely through the CNIS (Table 3). This implies that the attenuating portion of the Central North Island region may extend to the surface of the descending slab.

The average rate of anelastic attenuation for non-volcanic ray paths in the Eastern North Island region (Table 2) is only about -0.003 g/km. Thus the anelastic attenuation rate for paths entirely within the CNIS (0.007) is two to three times higher than the rate for non-volcanic paths.

DEPTH TERM

One expects that the addition of the depth term, and in particular, the station constant terms in the MY regression, would significantly improve the fit of the attenuation model. Table 2 and Figures 5 and 6 show that the addition of the terms has little effect on the original JB terms (except for the scaling factor).

From Table 2, we see that the value of the depth coefficient for the ENI deep region is less than that for the ENI shallow region. A smaller depth term implies less variation of attenuation with depth within an individual data set. Molas and Yamazaki (1995) suggest that the depth term may not only reflect the variation of the Q value, but also the scattering of seismic waves as they near the surface. As discussed by Abercrombie (1998), due to the closure of cracks within rocks with increasing pressure, attenuation is dependent on pressure with friction at cracks being the dominant mechanism of intrinsic attenuation. Abercrombie (1998) suggests therefore that scattering attenuation should decrease with increasing depth in the upper crust as fractures are major scatterers of seismic energy. The depth term for the ENI shallow data set is consistent with a decrease in attenuation with depth.

The depth coefficient of the CNID region for the non-volcanic data set is negative in value (Table 2), implying an increase in attenuation with depth. However it appears that the depth term is simply being substituted for part of the anelastic attenuation term because of the close correlation between depth and distance for the deep events.

TABLE 1: Distribution of data used for the regression analyses.

	No. of Events	No. of Records	Distance (km)	Depth (km)	Magnitude	Acceleration (m/s^2)
ENID						
Non - Volcanic	23	297	44 to 499	34 to 96	3.3 to 6.5	1.3e-06 to 0.0501
Volcanic	17	32	81 to 380	34 to 96	3.4 to 6.5	2.2e-06 to 0.0046
ENIS						
Non - Volcanic	29	342	28 to 493	9 to 33	3.1 to 5.1	1.2e-06 to 0.0076
Volcanic	19	45	70 to 388	9 to 33	3.3 to 5.1	1.7e-06 to 0.0005
CNID						
Non - Volcanic	31	286	137 to 499	104 to 275	3.7 to 5.5	1.2e-06 to 0.0024
Volcanic	16	41	109 to 300	104 to 228	3.8 to 5.5	1.6e-06 to 0.0002
CNIS						
Volcanic	18	44	20 to 449	5 to 33	3.3 to 5.4	2.1e-06 to 0.0061

TABLE 2: Attenuation coefficients for the non-volcanic data set.

Model*	**Constant**	**M**	**r**	$\log_{10}$ **r**	**Depth**
JB	c	a	b		
MY	b_0	b_1	b_2	b_3	b_4
		Eastern North Island Deep			
JB	-5.1941	0.9290	-0.0028	-1	-------
MY	-2.1716	0.9235	-0.0027	-1	0.0001
		Eastern North Island Shallow			
JB	-5.5615	0.9826	-0.0028	-1	-------
MY	-2.7833	0.9594	-0.0026	-1	0.0050
		Central North Island Deep			
JB	-5.6764	1.0049	-0.0018	-1	-------
MY	-2.6027	0.9036	-0.0011	-1	-0.0012

* Note that the coefficient of the $log_{10}\ r$ term has been constrained to –1 each case. Maximum accelerations are used for all models. [JB = Joyner and Boore (1981) model (in g). MY = Molas and Yamazaki (1995) model (in cm/s^2)]. Note that $|c-b_0|$ is, on average a constant term equal to $\log_{10}(980.7)$, hence the difference between the constant terms c and b_0 is largely due to the difference in units.

TABLE 3: Calculated anelastic attenuation rates for data with ray paths through the CNI. The travel paths were either partly through the ENI or CNID, or wholly (CNIS) within the shallow portion of the CVR.

Region	Attenuation
ENID	-0.0075
ENIS	-0.0081
CNID	-0.0072
CNIS	-0.0067

STATION TERMS

The station terms account for the fact that some stations have consistently greater or smaller PGA than that of the main trend. These differences are mainly due to site conditions, topographic variations and near-station path effects. Appendix 1 lists the station terms for each region for the MY type regressions for the non-volcanic data set. For example, the station MQZ is consistently much higher than the trend, particularly for the ENID (Figure 5, 6 and 7). It therefore has a much more positive station term than most other stations, as expected. Stations which lie much lower than the trend, likewise have negative station terms.

The values of the station coefficients are not consistent with those of the travel time corrections used by IGNS for earthquake location, i.e. low attenuation doesn't correlate with a small travel time correction. This suggests that the attenuation station terms include partial path effects as well as site effects. Comparisons between regions show that the attenuation station terms for individual stations are fairly consistent for different source regions except for a few stations (see Appendix 1).

The effect of the greater attenuation through the volcanic region was to a degree reflected in negative station terms for the NZNSN stations KUZ, MOZ, OIZ ,WLZ and Taupo Volcanic Zone deployment stations (Pancha, 1997). As seen from Figure 8, these stations lie well below the trend. Also note the scatter in the Taupo Volcanic deployment stations as previously mentioned. Station terms derived for these stations for earthquakes located within the CNID region were highly negative reflecting the difference between the low-attenuation slab paths and paths through the Central Volcanic Region.

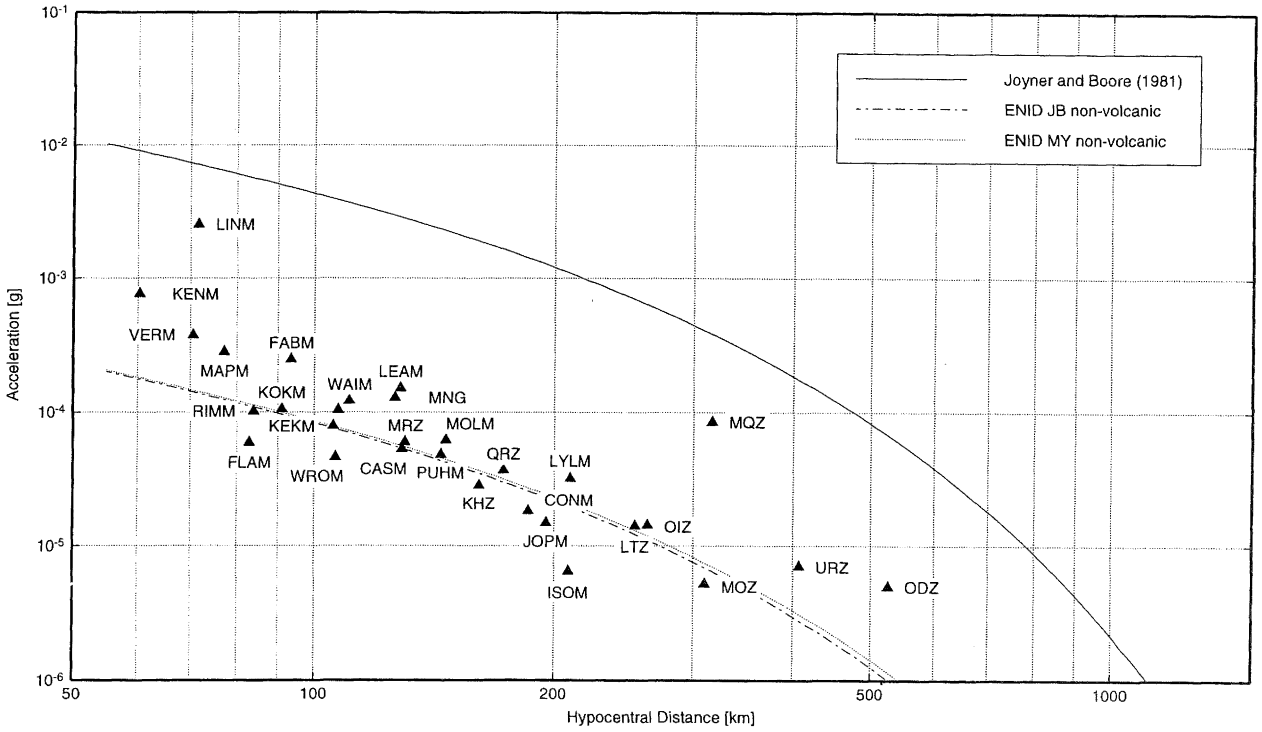

Figure 6: Comparison of the JB non-volcanic and the JB attenuation models with an ENID event of M_L = 3.6 and depth = 55 km. The difference in absolute level between these two models greatly increases at low magnitudes (compare with Figures 7 and 8), but the rate of anelastic attenuation is seen to be similar for the two models. The data also demonstrate the application of the MY station terms. Note that MQZ lies significantly above the main trend of the data. As seen in Appendix 1, MQZ has a highly positive station term to account for this, particularly for the ENID.

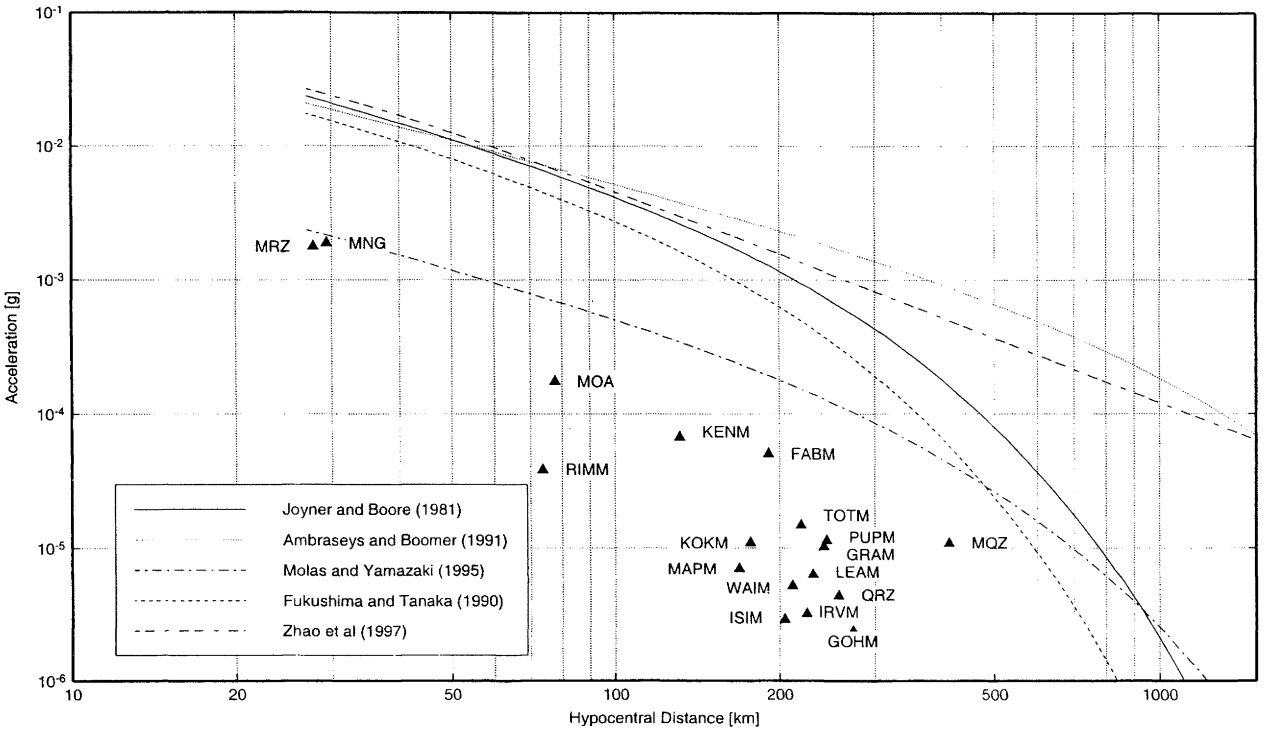

Figure 7: Comparison of the JB, Ambraseys snd Boomer (1991), MY, Fukushima and Tanaka (1990) and Zhao et al (1997) strong-motion models with data from an ENIS event of M_L = 3.6 and depth = 27 km. Those of the Japanese data set are more comparable to the New Zealand weak motion.

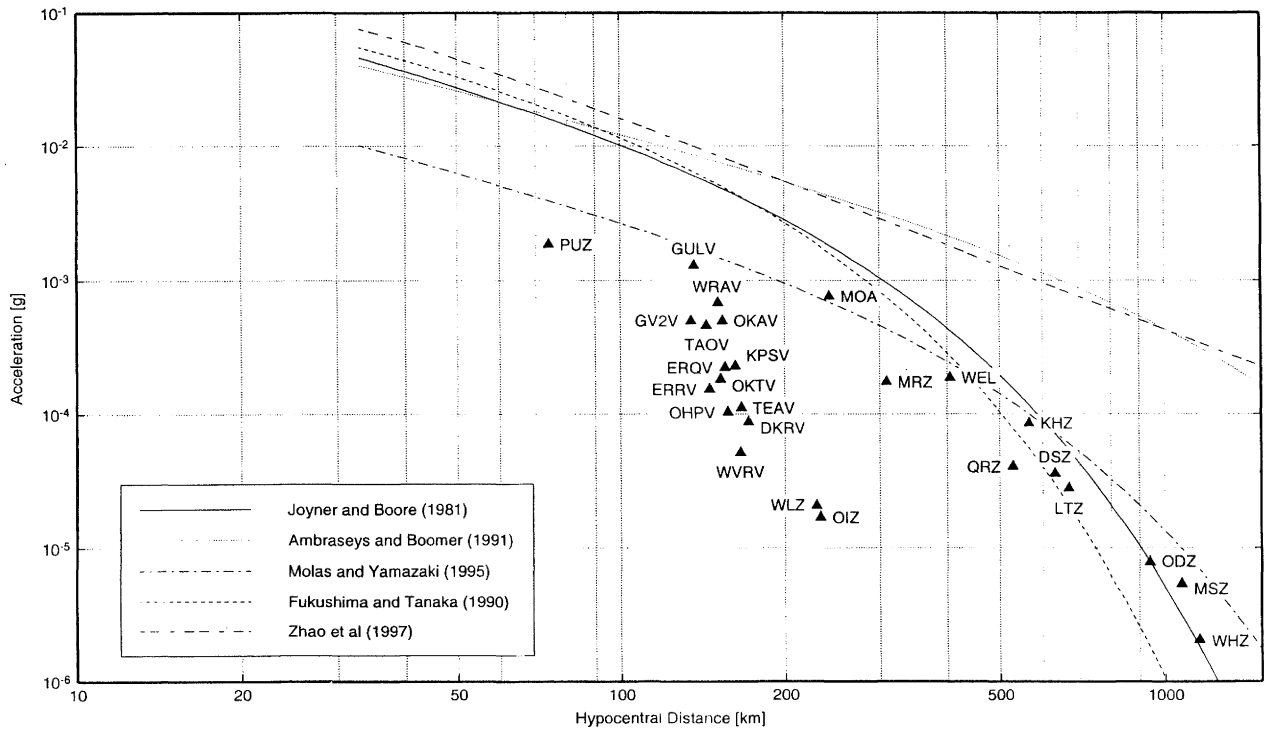

Figure 8: Comparison of the JB, Ambraseys and Boomer (1991), MY, Fukushima and Tanaka (1990) and Zhao et al (1997) strong-motion models with data from an ENIS event of M_L = 5.1 and depth = 33 km. Note the increasing improvement of the fit with increasing magnitude (compare with Figure 7). Note that the data from sites ending in "V" (the Taupo Volcanic deployment stations) and the NZNSN sites WLZ and OIZ are affected by volcanic paths. These station are part of the "volcanic" data set.

COMPARISON TO OVERSEAS AND NEW ZEALAND STRONG-MOTION RELATIONS

The strong motion relations were developed from data recorded in the near-field from large magnitude events (Table 4). This is in contrast to the weak-motion, low magnitude far-field data of this study. These two different data types may give rise to differences in the expected behavior of the resulting PGA. From the nonparametric description of peak accelerations above the Mexican subduction thrust, Anderson (1997) noted that the rate of decay of peak accelerations varied with respect to earthquake size. Accelerations from large earthquakes (M > 6) decreased more slowly with increasing distance from the site of energy release than accelerations from small earthquakes. Hadley and Helmberger (1980) also noted a decrease in the slope of the attenuation-distance relation with increasing magnitude. However, the rate of decrease of PGA is the same for JB as in the current study for the ENI (Tables 2 and 5 and Figure 6) so it is not clear how important this effect may be.

Table 4: Distribution of data used in the calculations of strong-motion attenuation relations.

Model	Acceleration (g)	Depth (km)	Distance (km)	Magnitude
Joyner and Boore (1981)	0.004 to 0.81	< 20	1.2 to 370	M_w = 5.0 to 7.7
Ambraseys and Boomer (1991)	0.001 to 0.99	≤ 25	1.0 to 313	M_s = 2.6 to 7.3
Fukushima and Tanaka (1990)	0.002 to 1.27	≤ 100	0.1 to 303	M_{JMA} ≥ 6.0
Molas and Yamazaki (1995)	>0.001	1 to 200	8 to 200	M_{JMA} = 4.0 to 8.0
Zhao *et al.* (1997)	0.0005 to 0.98	4 to 149	0.1 to 573	M_w = 5.1 to 7.4

TABLE 5: Attenuation relations within the literature.

	Model
Joyner and Boore (1981) *	$\log_{10} A = -1.02 + 0.249\ M - \log_{10} r - 0.00255\ r,\ r = d^2 + 7.3^2$
Ambraseys and Boomer (1991) *	$\log_{10} A = -1.09 + 0.238\ M - \log_{10} r - 0.0005\ r$
Molas and Yamazaki (1995) **	$\log_{10} A = 0.206 + 0.477\ M - \log_{10} r - 0.00144\ r - 0.00311\ h$
Fukushima and Tanaka (1990) **	$\log_{10} A = 1.30 + 0.41\ M - \log_{10} (r + 0.032 \cdot 10^{0.41 M}) - 0.0034\ r$
Zhao et al. (1997) * Model 5	$\log_{10} A = -0.409 + 0.331\ M - 1.59 \log_{10} (r^2 + 20^2)^{0.5} + 0.00566\ h$

* Accelerations are in g.

** Accelerations are in cm/s^2.

Comparisons between the weak motion data of this study have been made with attenuation models within the literature, including the recent New Zealand model (Zhao *et al.*, 1997), Japanese models (Fukushima and Tanaka, 1990; Molas and Yamazaki, 1995), the Western US (Joyner and Boore, 1981) and Europe (Ambraseys and Bommer, 1991). These strong motion relations are listed in Table 5. As seen in Figures 7 and 8, the MY model gives the closest fit to the data. A comparison of Tables 2 and 5 shows that the anelastic attenuation rate of the CNID region is similar to that determined for Japan by Molas and Yamazaki (1995). Moreover, the fit of the data improves as the magnitude of the events increases (Figures 7 and 8).

Figures 7 and 8 also show comparisons between the JB, Ambraseys and Bommer (1991) and Zhao *et al.* (1997) attenuation models with the weak motion data. The Zhao *et al.* (1997) Model 5 is used for the comparison as it takes no account of focal mechanism or site conditions. However, the Zhao *et al.* (1997) relation does not include an anelastic attenuation term. From Tables 2 and 5, and Figure 6 we can see that the rates of anelastic attenuation found for the ENI in this study are comparable to those of the tectonic regimes of Western US (Joyner and Boore, 1981), as mentioned above. Once again we see that the model improves with increasing magnitude (Figure 8).

The observed differences in absolute level, particularly at low magnitudes, between the strong-motion attenuation relations and those of weak-motion derived in this study may be the result of a number of factors. These include the difference between the magnitude and distance ranges of the strong- and weak-motion data, differences in frequency characteristics of large and small earthquakes, the difference

in characteristics of PGA between strong-motion, near-field data and the weak-motion far field data due to source effects, and differences in magnitude scales (M_L vs M_S or M_{JMA}). The difference is unlikely to be due to site effects even though the sites of this study are mostly sited on bedrock while those of the strong-motion studies are sited on a range of soil conditions. If site effects were the major cause of the observed difference in PGA level between the strong-motion and weak-motion relations, one would not expect the difference to scale with magnitude as observed here.

CONSIDERATION OF WAVE PROPAGATION

Attenuation relations describe the smooth decrease of ground motion with distance. However, these relations may require a more complex form to account for wave propagation through the crust. Many strong-motion studies have noted that at mid-field distances, amplitudes become constant in value and there appears to be an absence of geometric spreading. These large amplifications have been determined to be the result of post-critical reflections from either mid-crustal discontinuities, the subducting slab, or the base of the crust (Atkinson and Mereu, 1992; Atkinson, 1995). These reflections influence attenuation values at an average distance of about 50-150 km (e.g. Mori and Helmberger, 1996). The degree at which these reflections affect the observed ground-motion depends greatly on the local geological and velocity structure (Burger *et al.*, 1987; Mori and Helmberger, 1996), as well as focal depth (Somerville and Yoshimura, 1990; Atkinson, 1995). There should thus be a transition in the attenuation model between ground-motion dominated by direct arrivals at near-field distances to an interval at greater distances dominated by post-critical reflections (Burger *et al.*, 1987).

An interval of constant amplitude, due to post-critical reflections from crustal discontinuities, were not visually observed from the data of this study. This is due to insufficient data at distances of 50-150 km and/or to the fact that the data were not at sufficiently shallow depths. Simple ray tracing across the North Island show that most reflections, including those from the Moho, occur at distances of about 50-170 km. Most direct arrivals occur at distances less than 100 km, though shallow seismic sources transmit direct rays which extend to distances of the order of 100-200 km. The ray tracing indicated that the arrivals of this study are dominated by refractions from lower layers travelling in a north-south direction.

Similarly, the boundary of the highly attenuating material of the Central Volcanic Region could not be determined because of the lack of a closely spaced station distribution across the bounding regions. In order to determine the effects of direct and post-critical reflections on attenuation patterns, data across the whole distance spectrum is required.

AZIMUTHAL DEPENDENCE

The amplitude, attenuation rate and spectral response of peak ground accelerations have been found to be azimuthally dependent in other regions (Campbell, 1991; Campbell and Bozorgnia, 1994). Ray paths parallel to the geological structure of a region, the geological "grain", in general experience less attenuation, while ray paths oriented perpendicular to structures, such as fault zones, are attenuated to a greater extent (Campbell, 1991).

The azimuthal variation of PGA has not been investigated for New Zealand earthquakes, though the azimuthal variation of isoseismals has been studied (Smith, 1978, Smith, 1995; Kozuch *et al.*, 1996). Smith (1995) defined the ellipticity of isoseimals for three regions: the eastern North Island, Wellington-Marlborough and Canterbury. These ellipticities, defined as the N40E semi-axis divided by the N50W semi-axis, were 0.89, 1.21 and 0.74 respectively. For this study, the procedure of Kozuch *et al.* (1996) (see Appendix 2), designed to quantify the azimuthal variation in a sparse data set, has been adopted to examine the azimuthal dependence of PGA attenuation. The ENID, ENIS, CNID, and CNIS data sets were defined as in the previous sections, but data, including those of the temporary deployments, at all distances were used. An attempt was made to divide the Eastern North Island Deep and Shallow regions into north and south sections, but there were insufficient data for the separation.

The data for each region were divided into bins based on magnitude and acceleration values (Table 6). The magnitude and acceleration bins were combined to produce a total of 20 data bins for each region. For each region, a composite distance-azimuth plot of the data projected back to the "centre" (see Appendix 2) of the region was made. To overcome the bias due to an azimuthally uneven station distribution, the data were truncated at radial distances so that data were approximately evenly distributed at all azimuths. The truncation values were 700 km for the CNID, 625 km for the CNIS, 300km for the ENID region, and 375 km for the ENIS region.

TABLE 6: Criteria for binning data for analysis of azimuthal dependence with respect to acceleration and magnitude.

Acceleration (g)		
A1 = <	0.000001	
A2 = ≥	0.00001	and < 0.0001
A3 = ≥	0.0001	and < 0.001
A4 = ≥	0.001	

Magnitude		
3.0	≥ M1 <	3.5
3.5	≥ M2 <	4.0
4.0	≥ M3 <	4.5
4.5	≥ M4 <	5.0
5.0	≥ M5	

Although all of the 20 data bins for each region were considered, all but 9 were discarded because the bins either contained too few data, or the data were not evenly distributed over two adjacent quadrants. The shallow Central North Island region in particular had a very sparse data set. Table 7 lists the number of data points in each of the bins that contain sufficient data.

TABLE 7: Number of data per bin used for azimuthal analysis.

Bin	Region	Number of data points
A2.M4	CNIS	37
A1.M2	CNID	50
A1.M3	CNID	174
A2.M2	CNID	34
A2.M3	CNID	275
A3.M3	CNID	38
A2.M3	ENIS	86
A2.M4	ENIS	70
A2.M3	ENID	101
A3.M2	ENID	42
A3.M3	ENID	57
A3.M5	ENID	27

The major and minor axes of these bins are shown in Figure 9. Within the ENIS region, the major axes are oriented at 50-55° while the minor axes are oriented at about 140-145° (Figure 9). This differs slightly from those of the ENID region. Ellipses of the ENID region have major axes oriented at 35-40° and minor axes oriented at 125-130°. These differences are probably not significant.

The orientation of the minor axes (the direction of greatest attenuation) for all bins in the CNI region is about 115-125° from North. For bins with major and minor axes perpendicular to each other, the major axis is oriented at about 25-35°. For the two bins where the major and minor axes are not orthogonal (CNID A1M3 and A2M3), the major axis is oriented at about 50-55°. Such a distribution, where the major and minor axes are not perpendicular, may occur because earthquakes within this region originate in the subducting slab. Ray paths travelling longer distances through the slab will experience less attenuation than those travelling through the mantle. The orientation of this low attenuation path may be different from the low attenuation direction in the crust.

The orientation of the major axis of the one bin in the CNIS is 5°, while the minor axis is oriented at 95°. Thus there appears to be a difference in the azimuthal variation of attenuation for waves originating in the CNIS compared to all the other regions.

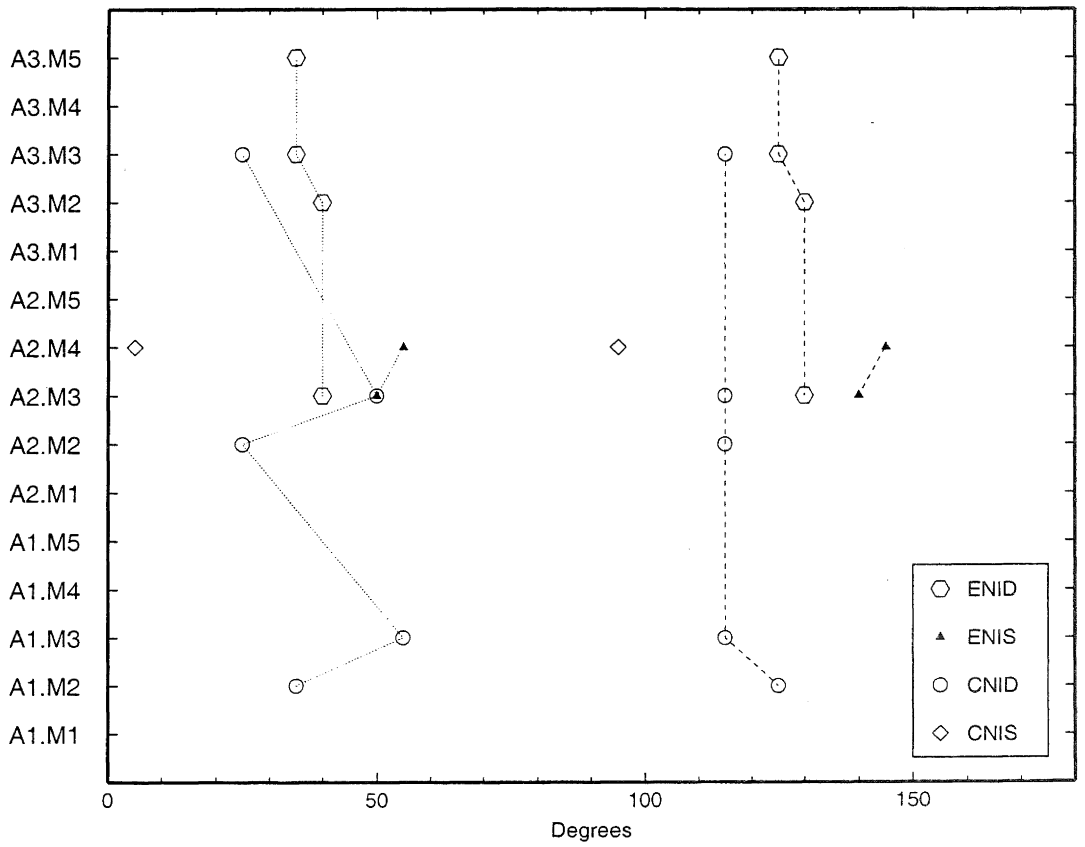

Figure 9: Plot of orientation of major (dotted line) and minor (dashed line) axes of ellipses determined for the CVR and ENI regions. Note that the CVRD A1M3 and A2M3 axes are not perpendicular to each other. Refer to Table 6 for bin definitions.

It is unclear whether the small differences between the azimuthal dependence of the Eastern North Island and deep Central North Island region are due to tectonic differences or are simply due to the sparse data. The orientation of the minor axes of the ENI and CNID are comparable, while slight differences in the orientation of the major axes of the CVRD and ENI may be due to the fact that earthquakes of the CNID originate deeper in the subducting slab.

The technique used to find the direction of the major and minor axes (Kozuch *et al.*, 1996) does not give the relative lengths of the axes. The ratio of major to minor axis length as estimated from a composite distance-azimuth plot of the data bins (Figure 10), varies from barely over 1 to about 2.5. A more precise way of quantifying the distribution is needed along with a higher density of data to determine the true level of the azimuthal variation in attenuation.

The orientation of the major axes within the Eastern North Island regions agree with the strike of the Hikurangi subduction zone and the predominant faults of the area. This is consistent with the findings of Kozuch *et al.* (1996) and Smith (1995). Differences exist, however, between the azimuthal dependence of attenuation determined in this study and that of Kozuch *et al.* (1996) for the CVR.

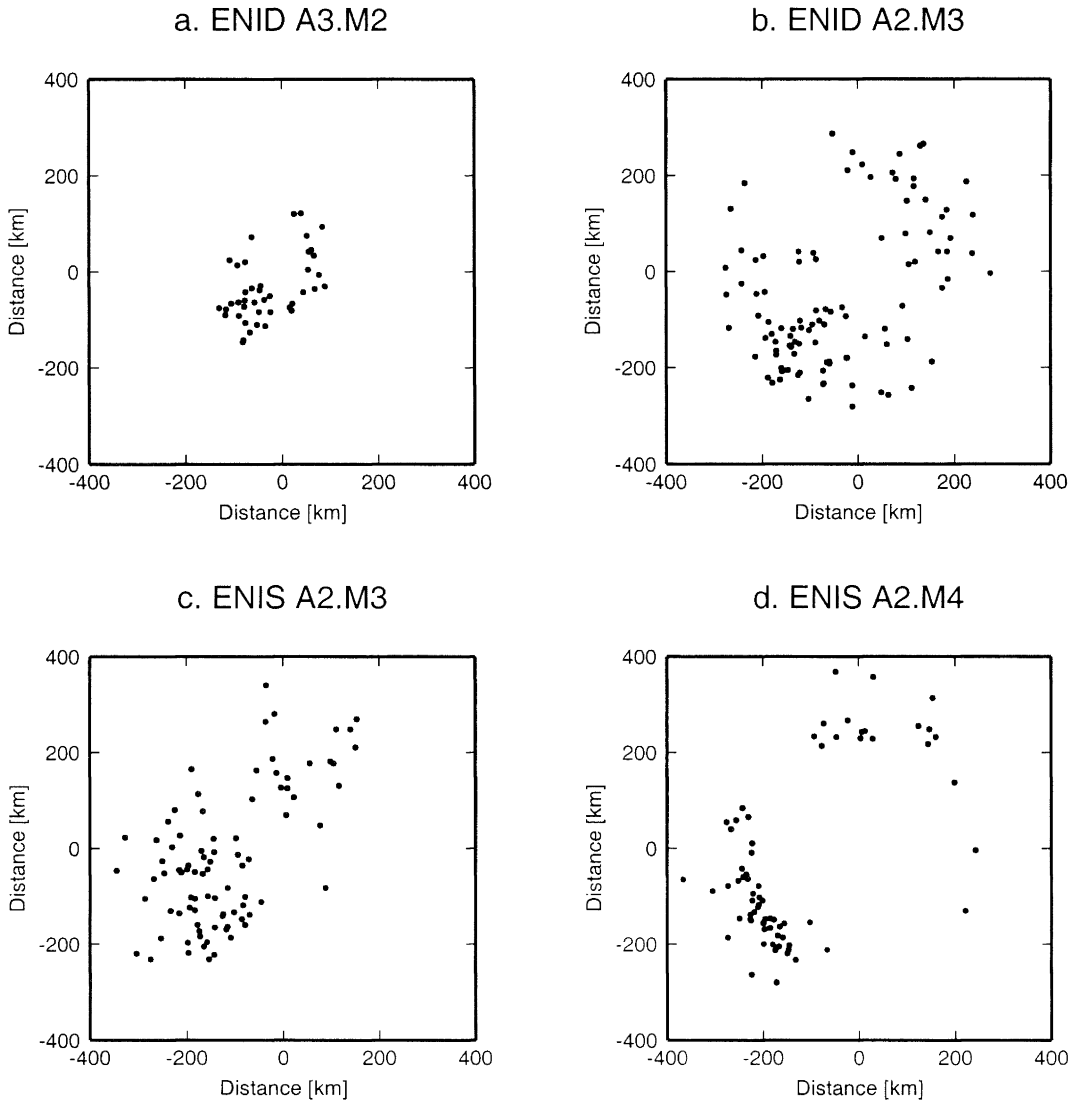

Figure 10: Composite projection of all stations to all earthquakes for data from four acceleration-magnitude data bins defined in Tables 6 and 7. Each point corresponds to the distance and azimuth from an earthquake to a station. In each case the earthquake location has been translated to (0,0) on the plot. As expected, as the magnitude is increased for a particular PGA (eg 17c to 17d), the distance at which that acceleration is observed is increased. A circular pattern would imply no azimuthal variation in attenuation.

Kozuch *et al.* (1996) observed no distinct azimuthal dependence within the CVR, whereas such a dependence was found for the CNI region of the current study. From this study it appears that both the highly attenuating material of the Central Volcanic Region and subducting Pacific Plate may have a directional influence on PGA attenuation and that these azimuthal influences may differ from those of the Eastern North Island.

DISCUSSION AND CONCLUSIONS

Regression analysis of peak ground accelerations of weak ground motions has allowed differences in attenuation rate between the Eastern and Central North Island regions to be quantified. The attenuation relations and rates were based on the source regions as well as the source-receiver path. As expected, it has been found that seismic waves which travel through the CVR are more attenuated than those through the subducting slab of the Pacific Plate and the overlying crust of the Australian Plate. The anelastic attenuation rate of seismic waves from deep earthquakes travelling exclusively through the CNI was found to be -0.007 g/km, while the rate for seismic waves from deep earthquakes travelling within the ENI region was of the order of -0.003 g/km. A similar rate of attenuation of -0.003 g/km was also observed for travel paths within the ENIS region. Thus, for the distance ranges considered in this study, the rate of attenuation from earthquakes occurring in the upper 33 km of the crust is comparable to earthquakes occurring below 33 km within the ENI region. This is a reasonable result considering the sub-crustal travel path for the majority of the earthquake-station pairs in these two groups. Attenuation rates of the CNID region for earthquakes originating within the slab which do not travel through the crust or mantle of the CNI region were found to be the lowest at a rate of –0.001 to -0.002 g/km. Seismic waves for these events spent a greater portion of the travel time within the subducted slab. This is consistent with the hypothesis that seismic waves travelling through the subducted Pacific Plate experience less attenuation than those travelling through the overlying crust. Seismic waves from shallow earthquakes, which travel solely within the CNI region experience the greatest amount of attenuation at a rate of -0.007 to –0.008 g/km.

The anelastic attenuation rate is similar for paths partly and solely in the CVR (as used in this paper), whereas it would be expected that the attenuation would be considerably greater for paths completely in the CVR. A possible explanation is that the permanent stations to the west of the CVR that have been included in the CNI data set (KUZ, MOZ) lie outside the zone of high attenuation. This would cause some of the CNIS volcanic paths to lie outside the zone of high attenuation and would reduce the anelastic attenuation term calculated in the regression. The similarity of the attenuation rate between the CNI deep and shallow volcanic data sets also suggests that the zone of high attenuation extends to the surface of the subducting slab.

The data set used in this study was insufficient to define the boundary between the attenuating zone of the CVR and that of the surrounding regions. However, since the commencement of this study, significantly more three-component data have been collected by the NZNSN and thus it will be soon possible to define the boundary. In addition, this study focused on events with large numbers of recording stations (an average of 11). With the increase in available data, it may be possible to improve coverage by including less well-recorded events. In particular, it would be beneficial if events recorded only by the stations within Taupo Volcanic Zone were also included in the data set.

On comparison with strong-motion relations, it was found that the weak-motion relations had the greatest similarities with Japanese models (Fukushima and Tanaka, 1990; Molas and Yamazaki, 1995). All of the strong-motion attenuation models significantly overestimate the absolute level of the weak-motion, particularly at low magnitudes. However, the rate of attenuation of the Eastern North Island weak-motion is comparable to the Western US JB model. These results show that attenuation rates of weak-motion data are similar to those of strong-motion and thus weak-motion attenuation may be useful in estimating relative rates of strong-motion attenuation.

Azimuthal dependence of PGA determined within the Eastern North Island region corresponds to that determined using isoseismals (Smith, 1995, Kozuch *et al.*, 1996), with the major axis oriented parallel to the strike of the subducting slab. An azimuthal dependence was also noted in the CVR contrary to the isoseismal study of Kozuch *et al.* (1996). The directional influence of PGA within the CNID region appears to be similar to that of the ENI region. Within the CNIS region, preferred directions appear to be influenced by the more northerly trending structures of the region (Grindley and Hull, 1986). The degree of azimuthal variation could not be determined using the method applied and further investigation with a larger data set and a more precise method is required to do so. A larger data set would also allow the determination of the boundaries of the highly attenuating region in the central North Island.

ACKNOWLEDGMENTS

We are very grateful for the use of data from the Institute of Geological and Nuclear Sciences earthquake catalogue. Much of the data used for this study was recorded by the National Seismograph Network. We also appreciate the many people at IGNS responsible for the collection of the additional data collected via temporary networks. These people include Tony Hurst, and especially the project leaders Martin Reyners, for the Marlborough and Eastern North Island deployments, and Hugh Bibby, for the TVZ deployment. Brian Dawkins provided significant statistical insight. The many helpful suggestions and comments from Mike Kozuch, Euan Smith, Rachel Abercrombie, Tim Stern, and Graeme McVerry and an unkown reviewer were much appreciated. We also wish to thank the Earthquake Commission for their financial support.

REFERENCES

Abercrombie, R. E. (1998), A summary of attenuation measurements from borehole recordings of earthquakes: the 10 Hz transition problem, *Pure and Applied Geophysics,* **153**, 475-487.

Ambraseys, N. N. and Boomer, J. J. (1991), The attenuation of ground accelerations in Europe, *Earthquake Eng. and Str. Dyn.*, **20**: 1179-1201.

Anderson, J. G. (1997), Nonparametric description of peak acceleration above a subduction thrust, *Seism. Res. Letters,* **68**(1): 86-93.

Atkinson, G. M. (1995), Attenuation and source parameters of earthquakes in the Cascadia Region, *Bull. Seism. Soc. Am.,* **85**(5): 1327-1342.

Atkinson, G. M. and Mereu, R. F. (1992), The shape of ground motion attenuation curves in southeastern Canada, *Bull. Seism. Soc. Am.*, **82**(3): 2014-2031.

Bolt, B. A. and Abrahamson, N. A.(1982), New attenuation relations for peak and expected accelerations of strong ground motion, *Bull. Seism. Soc. Am.,72*(6): 307-2321.

Burger, R. W., Somerville, P. G., Barker, J. S., Hermann, R. B. and Helmberger, D. V. (1987), The effect of crustal structure on strong ground motion attenuation relations in eastern North America, *Bull. Seism. Soc. Am.*, **77**(2): 420-439.

Campbell, K. W. (1981), Near-source attenuation of peak horizontal acceleration, *Bull. Seism. Soc. Am.*, **71**(6): 2039-2070.

Campbell, K. W. (1991), An empirical analysis of peak horizontal acceleration for the Loma Prieta, California, earthquake of 18 October 1989, *Bull. Seism. Soc. Am.*, **81**(5): 1838-1858.

Campbell, K. W. and Bozorgnia, Y. (1994), Empirical analysis of strong ground motion from the 1992 Landers, California, earthquake, *Bull. Seism. Soc. Am.*, **84**(3): 573-588.

Dowrick, D. J. (1991), A revision of attenuation relationships for Modified Mercalli intensity in New Zealand earthquakes, *Bull. N.Z. Nat. Soc. Earthquake Engineering.* **24**(3): 210-224.

Dowrick, D.J. and Sritharan, S. (1993a), Attenuation of peak ground accelerations in some recent New Zealand earthquakes, *Bull. N.Z. Nat. Soc. Earthquake Engineering*, **26**(1): 3-13.

Dowrick, D. J. and Srithanran, S. (1993b), Peak ground accelerations recorded in the 1968 Inangahua earthquake and some attenuation implications, *Bull. N.Z. Nat. Soc. Earthquake Engineering,* **26**(3): 349-355.

Draper, N. R. and Smith, H. (1981), *Applied Regression Analysis*, 2nd edition, Wiley and Sons, Inc.

Fukushima, Y and Tanaka, T. (1990), A new attenuation relation for peak horizontal acceleration of strong earthquake ground motion in Japan, *Bull. Seism. Soc. Am.*, **80**(4): 757-783.

Gledhil, K. R., Randall, M. J. and Chadwick, M. P. (1991), The EARSS digital seismograph: System description and field trials, *Bull. Seism. Soc. Am., 81*(4): 1380-1390.

Grindley, G. W. and Hull, A. (1986), Historical Taupo earthquakes and earth deformation, *R. Soc. N. Z. Bull.*, **24**: 173-186.

Hadley, D. M. and Helmberger, D. V. (1980), Simulation of strong ground motion, *Bull. Seism. Soc. Am., 70*(2): 617-630.

Haines, A. J. (1981), A local magnitude scale for New Zealand earthquakes, *Bull. Seism. Soc. Am.*, **71**(1): 275-294.

Hatherton, T. (1970), Upper mantle inhomogeneity beneath New Zealand: Surface manifestations, *J. Geophys. Res.*, **75**(2): 269-284.

Joyner, W. B. and Boore, D. M. (1981), Peak horizontal acceleration and velocity from strong-motion records including records from the 1979 Imperial Valley, California, earthquake, *Bull. Seism. Soc. Am.*, **71**(6): 2011-2038.

Kozuch, M. J. E., Smith, E. and Vere-Jones, D. (1996), Modeling New Zealand isoseismal shapes with a sire-specific attenuation dependence (abstract). *EOS, Trans. (1995 Fall Meeting Supplement),* **77**(46): F510.

Molas, G. L. and Yamazaki, F. (1995), Attenuation of earthquake ground motion in Japan including deep focus events, *Bull. Seism. Soc, Am.*, **85**(5): 1343-1358.

Mooney, H. M. (1970), Upper mantle inhomogeneity beneath New Zealand: seismic evidence, *J. Geophys. Res.*, **75**(2): 285-309.

Mori, J. and Helmberger, D. (1996), Large-amplitude Moho reflections (*SmS*) from Landers aftershocks, Southern California, *Bull. Seism. Soc. Am.*, **86**(6): 1845-182.

Pancha, A (1997), *Weak motion attenuation of the North Island, New Zealand*, Masters thesis, School of Earth Sciences, Victoria University of New Zealand, 128p.

Satake, K. and Hasida, T. (1989), Three-dimensional attenuation structure beneath North Island, New Zealand, *Tectonophysics*, **159**: 181-194.

Smith, W. D. (1978), Spatial distribution of felt intensities for New Zealand earthquakes, *N. Z. J. of Geol. Geophys.*, **21**(3): 293-311.

Smith, W. D. (1995), A development in the modelling of far-field intensities, *Bull. N.Z. Nat. Soc. Earthquake Engineering,* **28**(3): 196-217.

Smith, W. D. and Berryman, K. R. (1983), Revised estimates of earthquake hazard in New Zealand, *Bull. N.Z. Nat. Soc. Earthquake Engineering,* **16**(4): 259-272.

Somerville, P .and Yoshimura, J. (1990), The influence of critical Moho reflections on strong ground motion recorded in San Francisco and Oakland during the 1989 Loma Prieta earthquake, *Geophys. Res. Letters,* **17**(8): 1203-1206.

Zhao, J. X., Dowrick, D. J. and McVerry, G. H. (1997), Attenuation of peak ground accelerations in New Zealand earthquakes, *Bull. N.Z. Nat. Soc. Earthquake Engineering,* **3**(2): 133-158.

APPENDIX 1. Station corrections for the non-volcanic data sets calculated using the maximum PGA.

Station	ENID	ENIS	CNID
CASM	-0.3.016	-0.2096	-0.2891
CLAM	-0.1539	-0.1700	-0.2766
COMN	-0.2247	-0.5351	0.0882
DSZ	-0.1943	-0.3567	0.0694
FABM	0.3131	0.2665	0.1183
FLAM	-0.3134	-------	-------
GOHM	-0.0148	-0.0859	0.1721
GRAM	0.2410	0.2336	-0.0080
IRVM	-0.2646	-0.2292	-0.3925
ISIM	-0.2893	-0.2565	-0.3403
ISOM	-0.4675	-0.6261	-------
JOPM	-0.1289	-------	-------
KEKM	-0.2806	-0.2210	0.1378
KENM	0.4575	0.3993	0.1867
KHZ	-0.1323	-0.0602	0.2620
KOKM	-0.1165	-0.0391	-0.2262
LEAM	0.2573	0.2227	-0.0354
LINM	1.2231	-------	-------
LTZ	-0.1858	-0.3090	-0.1930
LYLM	0.0104	-0.1135	0.0026
MAPM	-0.1571	-0.0948	-0.1232
MNG	0.0951	0.3895	0.5232
MOA	0.3912	0.5123	0.6827
MOLM	-0.0808	-0.1232	-0.2161
MQZ	0.9250	0.7399	-------
MRZ	0.0496	0.3191	-0.3287
NMCM	-0.3042	-0.1977	-------
PUHM	-0.0793	-0.3091	-0.0141
PUPM	0.2872	0.3768	-0.0712
PUZ	-0.4230	-0.1175	-0.2542
QRZ	-0.0327	-0.0361	-0.3375
RIMM	-0.1145	0.0199	-0.1784
SPCM	-0.0594	0.0442	-------
SRWM	-0.0828	-0.1152	-0.0864
TOTM	0.4747	0.3481	0.1931
URZ	-0.2078	-0.2002	-0.1333
VERM	0.3866	-------	-------
WAIM	-0.0348	-0.0664	-0.1746
WEL	-0.0399	0.4592	0.4761
WROM	-0.1646	0.1408	0.1092
WVZ	-0.1635	-------	-------

Appendix 2

The assumption has been made that all earthquakes within a specific region and bin produce azimuthally similar attenuation patterns (Figure A2.1a), i.e. the effect of source mechanisms has been ignored. For each earthquake-station pair, the distance and azimuth were used to project the origin back to a common point at the centre of the region (Figure A2.1b). An ellipse was then fitted to the data.
To maximise the use of limited data, data points within a single bin were projected onto a rotating x axis (Kozuch *et al.*, 1996)(Figure A2.1c). The orientation of the minimum and maximum axes of the ellipse described by the data was then determined from the resulting plot (Figure A2.2). The procedure was first tested using an ellipse of known shape to determine the limits of the technique. It was found that the data must be evenly distributed over two adjacent quadrants to accurately describe an ellipse and must contain random scatter. While the direction of major and minor axes of the distribution are correctly determined, the ratio of the length of the major and minor axes does not give the true ellipticity.

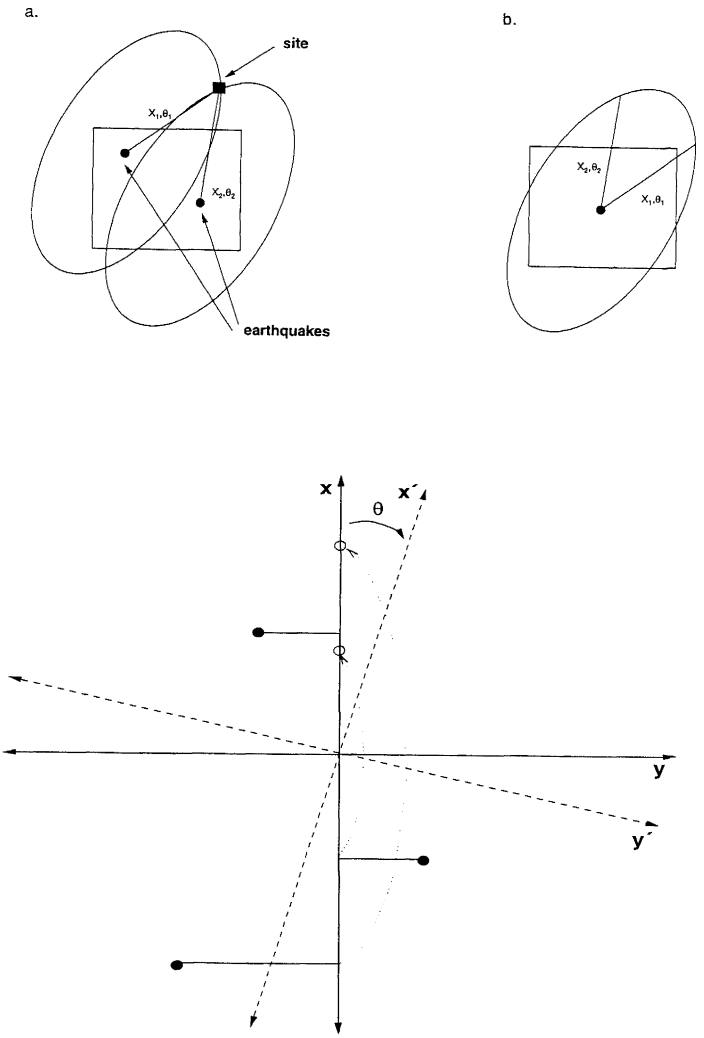

Figure A2.1: Procedure for determining azimuthal dependence. In a., the assumption is made that all earthquakes originating within a specific seismogenic region, represented by the grid cell, produce similar PGA attenuation patterns. Distance and azimuthal data of each earthquake-station pair are used to project the origin back to a common centre point at the "centre" of the region, as shown in b. The resultant ellipse depicted by the projection of each earthquake back to a centre point describes the average PGA that one should observe from any earthquake within the region of interest. To maximise the use of limited data, the data rotation procedure of Kozuch et al (1996) is employed to determine azimuthal dependence as shown in c. Data are projected onto the x axis. They are then folded onto the positive x quadrant. The axes are then rotated by an increment, θ, and the mapping of data back onto the positive x quadrant is repeated. The process of rotation and folding of data is iterated until 180° is completed. Because of symmetry, 360° of rotation is not required. For this study, θ is 5°.

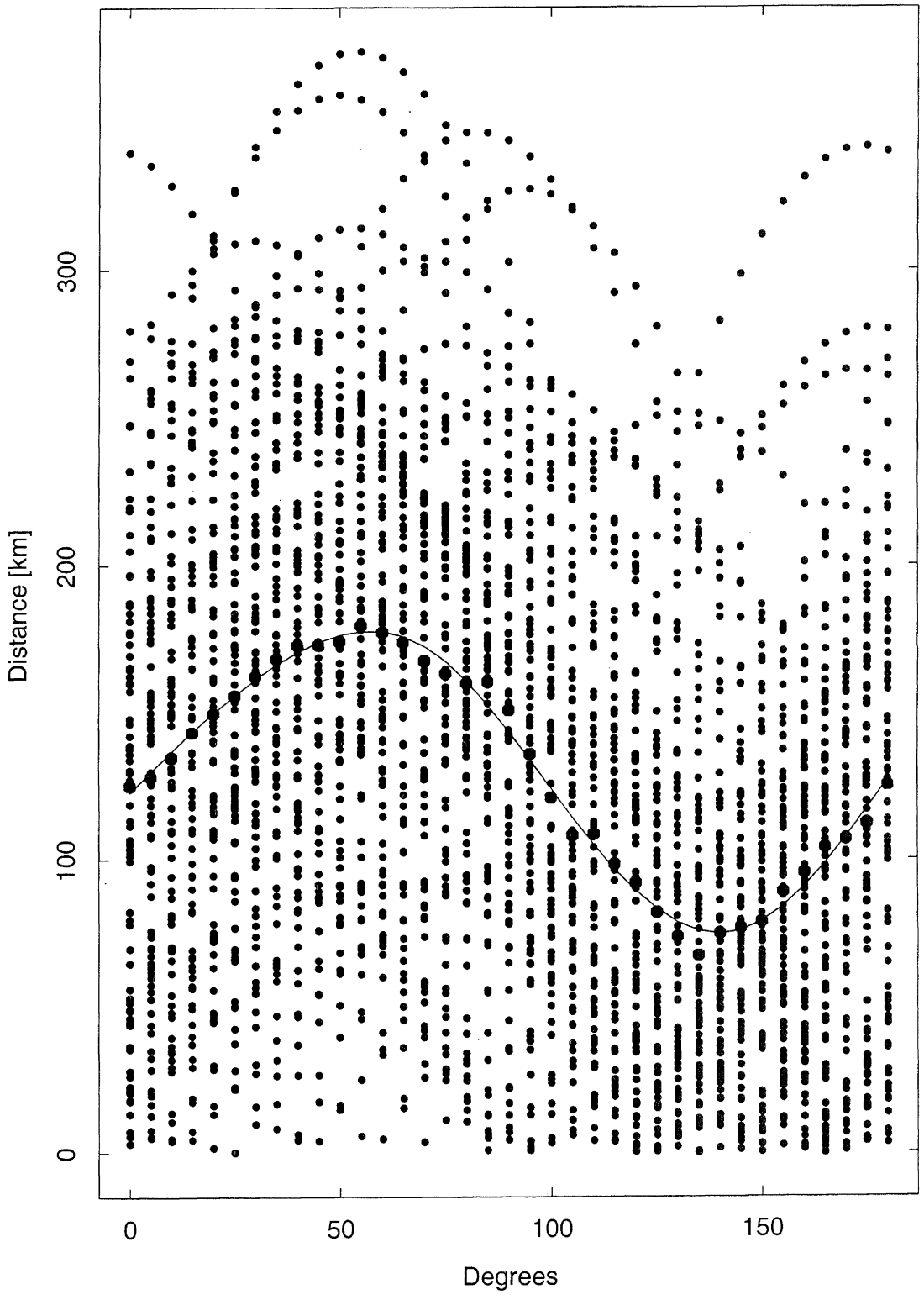

Figure A2.2: Plot of data from the ENIS A2M3 data bin. Data obtained through rotating the axes and mapping data points onto the positive x axis are plotted against the degree of rotation. For this study the increment of rotation was 5°. The median data value for each increment of rotation has been superimposed on the plot (large dots) as well as a smoothed fit to these points (solid line). Both the fitted curve and the median points were used to help determine the major and minor axes and their orientation. In this example, the major axis is oriented at 50° with a length of 180 km. The minor axis is oriented 90° to the major axis at 140° with a length of 70 km. The ratio of the lengths of axes in the figure does not give the true ratio of the lengths of the major and minor axes of the ellipse.